ISSN 2644-3260 (online)

Artificial Intelligence in *Medical Imaging*

Continuous Publication Volume 5 Number 1 September 28, 2024

Published by Baishideng Publishing Group Inc

AIMI

Artificial Intelligence in Medical Imaging

Contents

Continuous Publication Volume 5 Number 1 September 28, 2024

ORIGINAL ARTICLE

Retrospective Study

LETTER TO THE EDITOR

Contents

Continuous Publication Volume 5 Number 1 September 28, 2024

ABOUT COVER

Editorial Board Member of *Artificial Intelligence in Medical Imaging*, Nesreen Mohamed Mohey, MD, Professor, Department of Radiodiagnosis, Zagazig University, Zagazig, Eastern Province, Egypt.
nesreenmohey77@yahoo.com

AIMS AND SCOPE

The primary aim of *Artificial Intelligence in Medical Imaging* (*AIMI*, *Artif Intell Med Imaging*) is to provide scholars and readers from various fields of artificial intelligence in medical imaging with a platform to publish high-quality basic and clinical research articles and communicate their research findings online.

AIMI mainly publishes articles reporting research results obtained in the field of artificial intelligence in medical imaging and covering a wide range of topics, including artificial intelligence in radiology, pathology image analysis, endoscopy, molecular imaging, and ultrasonography.

INDEXING/ABSTRACTING

The *AIMI* is now abstracted and indexed in Reference Citation Analysis, China Science and Technology Journal Database.

RESPONSIBLE EDITORS FOR THIS ISSUE

Production Editor: *Hua-Ge Yu*; **Production Department Director:** *Xu Guo*; **Cover Editor:** *Yun-Xiaojiao Wu*.

NAME OF JOURNAL
Artificial Intelligence in Medical Imaging

ISSN
ISSN 2644-3260 (online)

LAUNCH DATE
June 28, 2020

FREQUENCY
Continuous Publication

EDITORS-IN-CHIEF
Caroline Chung, Guo-Lin Ma, Jun Shen

EDITORIAL BOARD MEMBERS
https://www.wjgnet.com/2644-3260/editorialboard.htm

PUBLICATION DATE
September 28, 2024

INSTRUCTIONS TO AUTHORS
https://www.wjgnet.com/bpg/gerinfo/204

GUIDELINES FOR ETHICS DOCUMENTS
https://www.wjgnet.com/bpg/GerInfo/287

GUIDELINES FOR NON-NATIVE SPEAKERS OF ENGLISH
https://www.wjgnet.com/bpg/gerinfo/240

PUBLICATION ETHICS
https://www.wjgnet.com/bpg/GerInfo/288

PUBLICATION MISCONDUCT
https://www.wjgnet.com/bpg/gerinfo/208

ARTICLE PROCESSING CHARGE
https://www.wjgnet.com/bpg/gerinfo/242

STEPS FOR SUBMITTING MANUSCRIPTS
https://www.wjgnet.com/bpg/GerInfo/239

ONLINE SUBMISSION
https://www.f6publishing.com

Artificial Intelligence in Medical Imaging

Submit a Manuscript: https://www.f6publishing.com

Artif Intell Med Imaging 2024 September 28; 5(1): 93993

DOI: 10.35711/aimi.v5.i1.93993

ISSN 2644-3260 (online)

ORIGINAL ARTICLE

Retrospective Study

Preoperative perineural invasion in rectal cancer based on deep learning radiomics stacking nomogram: A retrospective study

Zhi-Chun Zhao, Jia-Xuan Liu, Ling-Ling Sun

Specialty type: Oncology

Provenance and peer review: Unsolicited article; Externally peer reviewed.

Peer-review model: Single blind

Peer-review report's classification

Scientific Quality: Grade B
Novelty: Grade B
Creativity or Innovation: Grade B
Scientific Significance: Grade B

P-Reviewer: Teklemariam TA

Received: March 9, 2024
Revised: August 27, 2024
Accepted: September 5, 2024
Published online: September 28, 2024
Processing time: 200 Days and 23 Hours

Zhi-Chun Zhao, Jia-Xuan Liu, Department of Interventional Radiology, The First Affiliated Hospital of China Medical University, Shenyang 110000, Liaoning Province, China

Ling-Ling Sun, Department of Radiology, The fourth Affiliated Hospital of China Medical University, Shenyang 110032, Liaoning Province, China

Corresponding author: Jia-Xuan Liu, MD, Doctor, Department of Interventional Radiology, The First Affiliated Hospital of China Medical University, Heping District, Shenyang 110000, Liaoning Province, China. 3304352470@qq.com

Abstract

BACKGROUND

The presence of perineural invasion (PNI) in patients with rectal cancer (RC) is associated with significantly poorer outcomes. However, traditional diagnostic modalities have many limitations.

AIM

To develop a deep learning radiomics stacking nomogram model to predict preoperative PNI status in patients with RC.

METHODS

We recruited 303 RC patients and separated them into the training (n = 242) and test (n = 61) datasets on an 8: 2 scale. A substantial number of deep learning and hand-crafted radiomics features of primary tumors were extracted from the arterial and venous phases of computed tomography (CT) images. Four machine learning models were used to predict PNI status in RC patients: support vector machine, k-nearest neighbor, logistic regression, and multilayer perceptron. The stacking nomogram was created by combining optimal machine learning models for the arterial and venous phases with predicting clinical variables.

RESULTS

With an area under the curve (AUC) of 0.964 [95% confidence interval (CI): 0.944-0.983] in the training dataset and an AUC of 0.955 (95%CI: 0.900-0.999) in the test dataset, the stacking nomogram demonstrated strong performance in predicting PNI status. In the training dataset, the AUC of the stacking nomogram was greater than that of the arterial support vector machine (ASVM), venous SVM, and CT-T stage models (P < 0.05). Although the AUC of the stacking nomogram was greater than that of the ASVM in the test dataset, the difference was not

particularly noticeable (P = 0.05137).

CONCLUSION
The developed deep learning radiomics stacking nomogram was effective in predicting preoperative PNI status in RC patients.

Key Words: Rectal cancer; Perineural invasion; Radiomics; Deep learning; Machine learning

Core Tip: Four machine models (support vector machine, k-nearest neighbor, multilayer perceptron, and logistic regression) were used to predict the preoperative rectal cancer (RC) presence of perineural invasion (PNI) status, with good performance in both the arterial and venous phases. With an area under the curve of 0.964 in the training dataset and 0.955 in the test dataset, the stacking nomogram model to predict pretreatment PNI status had high predictive power and clinical utility, which can help diagnostic and treatment decision-making. Deep learning radiomics stacking models are rare in our RC PNI, which was also an innovation in our research.

Citation: Zhao ZC, Liu JX, Sun LL. Preoperative perineural invasion in rectal cancer based on deep learning radiomics stacking nomogram: A retrospective study. *Artif Intell Med Imaging* 2024; 5(1): 93993
URL: https://www.wjgnet.com/2644-3260/full/v5/i1/93993.htm
DOI: https://dx.doi.org/10.35711/aimi.v5.i1.93993

INTRODUCTION

Rectal cancer (RC) is the most common type of gastrointestinal cancer worldwide, and its incidence and mortality are steadily increasing, posing a severe threat to human health[1]. The two most distinguishing biological activities of malignant tumors are invasion and metastasis. Oncologists and physicians are becoming more aware of neural invasion in addition to the usual direct invasion, lymph node metastasis, and hematogenous metastasis.

One obvious method by which cancer cells spread is through neural invasion, also known as perineural invasion (PNI), which is the invasion of tumor cells around or through nerve fibers[2]. PNI is present in many different tumor types, including pancreatic ductal adenocarcinoma, gastric cancer, colorectal cancer, and prostate cancer. It plays a significant role in determining the pathological features and prognosis of malignant tumors by foretelling a high incidence of metastatic tumors, poor prognosis, and high rate of local recurrence[2,3]. PNI has a significant role in deciding whether patients benefit from postoperative chemotherapy and neoadjuvant chemoradiation[4-6]. Furthermore, it significantly affects the prognosis of individuals with rectal cancer who will survive over the long term. Therefore, physicians can benefit from knowing PNI status beforehand.

Traditional radiological methods, such as computed tomography (CT) and magnetic resonance imaging (MRI), do not determine the PNI status of rectal cancer. However, because RC is a temporally and spatially heterogeneous disease, the risk of invasive sampling and potential complications limit its application in tumor progression and real-time monitoring. As a result, a simple and noninvasive strategy to provide this critical information before clinicians make clinical treatment decisions must be developed.

Radiomics, which uses a large number of objective and quantitative imaging features to select imaging markers that are most closely related to clinical, pathological, molecular, and genetic characteristics, and then uses machine learning and statistical modeling to perform further quantitative analysis and analyze the correlation with clinical features, can noninvasively reflect tumor heterogeneity[7-9]. Several recent studies[10] have demonstrated that radiomics is a superior method for predicting PNI status in colorectal cancer. Guo *et al*[10] created a nomogram based on CT score and T2-weighted imaging score to predict PNI status in RC, and it performed the best [training set, area under the curve (AUC) = 0.906; test set, AUC = 0.884][11]. The results of the study demonstrated that radiomics can supplement conventional imaging techniques and aid physicians in decision-making. Additionally, a type of deep learning neural network that learns from the data itself is the convolutional neural network (CNN). Convolution is its central layer and is mostly utilized for segmentation, classification, and image recognition. Large data sets can be processed and the outcome of data analysis can be predicted and classified[12]. It is rarely stated that deep learning radiomics can be used to predict PNI status in RC.

Therefore, in this study, radiomics features of arterial and venous phases were extracted from enhanced CT images of patients with RC, and a deep learning radiomics nomogram was constructed to explore its application the prediction of PNI.

MATERIALS AND METHODS

Patients

Patients with RC who underwent enhanced CT examination at our hospital between March 2018 and December 2023 were included in this study retrospectively. The following were the inclusion criteria for patients (Figure 1): (1) Pathologically confirmed RC with PNI status; (2) Within 2 wk prior to surgery, an enhanced abdominal CT scan was conducted; and (3) All clinical information and pertinent laboratory results were recorded, including age, sex, history of alcohol consumption and smoking, carcinoembryonic antigen (CEA), carbohydrate antigen (CA) 19-9, routine blood tests, blood lipids, and T stage of the CT report. Exclusion criteria were (Figure 1): (1) Neoadjuvant chemoradiotherapy prior to surgery; (2) Complicated malignant tumors at other sites; and (3) Inadequate clinical data or poor image quality. Ultimately, the study comprised 303 patients (mean age 65.94 ± 10.76 years, age range 24-91 years; 165 male and 117 female). The patients were assigned to training (n = 242) and test (n = 61) datasets.

Spiral CT (Philips iCT 256) showed that all patients had enhanced abdominal scans with the following settings: Matrix 512 × 512, transverse fault thickness of 5 mm, pitch 0.5 s, tube voltage 120 kV, and tube current autoregulation. Patients in the supine position were injected with 80-100 mL (300 mg mL) at a rate of 3.0 mL/s with a delay of 30-35 s and 60-70 s, resulting in arterial and venous phase images.

Two seasoned radiologists who were blind to all clinical and pathological data evaluated the CT reported T stage (CT-T stage) using CT-enhanced images (Table 1).

Features for extraction and selection

Using the open-source 3D Slicer software (www.3D-Slicer.com, version 4.13.2), two radiologists manually identified and separated main tumors from axial CT scans at arterial and venous stages. The pixel intensity was normalized to transform the images to standardized inputs, which had the intensity range from 1024 to 1024 HU and the unified abdominal window (window level 50 and window width 350). The two radiologists repeated manual segmentation on the same group of 50 CT images to test the consistency of the two, intraclass correlation coefficients (CCs) used for consistency within the tester. For intraclass CCs used for consistency between examiner and assessors, only intraclass CCs > 0.75 indicated that acceptable stability of the construction model. Regions of interest (ROIs) include tumor and necrosis, bleeding areas and avoid the use of intestinal gases and contents. Fir every patient, two ROIs (venous and arterial phases) were created.

CT images were resampled to the voxel size of 1 mm × 1 mm × 1 mm. The raw images were processed using log, exponential, square, square root, gradient, and high wavelet transform and low wavelet filter. First-order features (n = 342), shape features (n = 14), gray-level dependence matrix (n = 266), gray-level size zone matrix (GLSZM, n = 304), and gray-level run-length matrix (n = 306) were among the radiomics features.

For the extraction of deep learning features, we initialized deep CNNs (DCNNs) using the pretrained weights in ImageNet, and selected the maximum cross-sectional area and its upper and lower images as three-channel images. The CT images were cropped using a rectangular ROI around the tumor contours. The size of the tumor patch was adjusted to 224224 to meet the input size requirements of the pretrained CNN model. We used the same normalization technique as in the ImageNet dataset, subtracting the mean (0.485, 0.456 and 0.406) and dividing by the standard deviation (0.229, 0.224 and 0.225) to ensure that the input features of the image agreed with the mean and standard deviation during ImageNet training.

We constructed two different deep learning models (DCNNs) for the deep learning feature extraction of tumor ROI in the arterial and venous stage CT images, respectively. The DCNN model was based on the Resnet-50 backbone, extracted deep learning features for classification, and predicted the RC PNI status based on a large number of 2D patches extracted from the ROI of the main cohort. The largest cross-sectional area and its upper and lower cross-section lesions were selected from the arterial and venous stages of the ROI as the input model, and the CT slices of the extracted features were input into the hierarchical convolution structure of the DCNN, using its CNN structure and learning weights on ImageNet, to obtain accurate ROI features in the average pool layer of the DCNN using the ResNet50 architecture. Using the average pool layer of ResNet-50 as the output of feature extraction generated a fixed size feature vector (usually 2048 dimensions), which provided a uniform and stable input feature for subsequent classification tasks, reducing the variability brought by different ROI sizes. The feature representation of this layer summarized the information about the entire ROI, providing a fixed-length feature vector suitable for subsequent classification tasks. We also froze most or all of the convolutional layers, only fine-tuning them in the final fully connected layer. This reduced the training time while maintaining the stability of the pretraining features.

Following the segmented ROI, 3696 features were extracted from each arterial and venous phase ROI, consisting of 2048 deep learning features and 1648 radiomics features, respectively. All features were normalized to a standard numerical range. We assessed the stability of two radiologists' tumor delineation using the interclass CC)/intraclass CC in order to remove unstable features and keep features with intraclass CC > 0.75. The Mann–Whitney U test (P < 0.05) eliminated the duplicate features. The features with the highest correlation with the outcome but the lowest correlation among the features were chosen using the maximum correlation and the minimum redundancy (mRMR). We selected the lambda value that yielded the least amount of error as the final parameter. LASSO regression lowered the coefficient of 0 and prevented overfitting and multicollinearity of the model when combined with fivefold cross-validation. The study flow chart, which includes image preprocessing, feature extraction, feature selection, and model building, is depicted in Figure 2.

Table 1 Statistical analysis results of clinical characteristics, *n* (%)

Characteristics	Training set (*n* = 242)		*P* value	Test set (*n* = 61)		*P* value
	PNI (*n* = 148)	PNI$^+$ (*n* = 94)		PNI (*n* = 40)	PNI$^+$ (*n* = 21)	
Age, (mean ± SD) (years)	67.01 ± 10.57	64.26 ± 12.06	0.063	67.33 ± 8.18	63.104 ± 8.66	0.065
Gender			0.248			0.86
Male	85 (58.2)	54 (39.1)		20 (64.5)	11 (35.5)	
Female	63 (65.6)	33 (34.4)		20 (66.7)	10 (33.3)	
Smoking			0.882			0.396
No	101 (60.8)	65 (39.2)		29 (69.0)	13 (31.0)	
Yes	47 (51.8)	29 (38.2)		11 (57.9)	8 (42.1)	
HGB (g/L)	126.98 ± 20.67	130.69 ± 20.00	0.071	128.881 ± 14.16	128.67 ± 22.28	0.965
RBC (10^{12}/L)	4.28 ± 0.62	4.40 ± 0.44	0.126	4.40 ± 0.47	4.28 ± 0.48	0.339
WBC (10^9/L)	6.55 ± 1.79	6.84 ± 2.19	0.265	6.18 ± 1.68	6.54 ± 1.67	0.391
PLT (10^9/L)	229.14 ± 77.31	240.92 ± 76.73	0.248	231.05 ± 70.18	231.62 ± 50.56	0.974
Lymphocyte(10^9/L)	1.61 ± 0.59	1.63 ± 0.68	0.808	1.59 ± 0.68	1.71 ± 0.95	0.567
Monocyte(10^9/L)	0.46 ± 0.23	0.47 ± 017	0.667	0.40 ± 0.14	0.70 ± 1.02	0.1
Neutrophil(10^9/L)	4.27 ± 1.55	4.54 ± 1.94	0.243	3.96 ± 1.51	4.47 ± 1.70	0.228
TG	1.47 ± 1.11	1.31 ± 0.60	0.18	1.43 ± 0.72	1.59 ± 0.98	0.502
Cholesterol	4.58 ± 0.88	4.72 ± 0.98	0.232	4.82 ± 0.89	4.91 ± 1.08	0.707
HDL	1.12 ± 0.28	1.19 ± 0.32	0.088	1.42 ± 1.51	1.13 ± 0.24	0.392
LDL	2.79 ± 0.69	2.93 ± 0.85	0.164	2.96 ± 0.84	3.18 ± 1.09	0.392
AproA	1.24 ± 0.19	1.26 ± 0.20	0.406	1.29 ± 0.17	1.22 ± 0.15	0.126
AproB	0.89 ± 0.19	0.90 ± 0.22	0.795	0.94 ± 0.18	0.89 ± 0.19	0.279
CEA (≥ 5 ng/mL)			**0.016**			0.173
No	94 (67.6)	45 (32.4)		28 (71.8)	11 (28.2)	
Yes	54 (52.4)	49 (47.6)		12 (54.5)	10 (45.5)	
CA19-9 (≥ 37 U/mL)			**0.003**			0.052
No	136 (64.8)	74 (35.2)		37 (71.2)	15 (28.8)	
Yes	12 (37.5)	20 (62.5)		3 (33.3)	6 (66.7)	
CT T stage			**0.000**			**0.006**
1/2	29 (85.3)	5 (14.7)		16 (88.6)	2 (11.1)	
3	73 (66.4)	37 (33.6)		17 (68.0)	8 (32.0)	
4	46 (46.9)	52 (53.1)		7 (38.9)	11 (61.1)	

CEA: Carcinoembryonic antigen; CA19-9: Carbohydrate antigen 19-9; $P < 0.05$.

Construction and evaluation of the predictive models

Preoperative PNI status was developed in the radiomics models (arterial and venous phase) using four machine learning models: Support vector machine (SVM), logistic regression (LR), multilayer perceptron (MLP), and k-nearest neighbor (KNN). The effectiveness of these four machine learning models in determining PNI status was assessed using the AUC and receiver operating characteristic (ROC) curves. We chose the most effective machine learning model by using the DeLong test to determine whether there were significant differences between the four distinct ROC curves.

For continuous clinical factors (age, blood routine index, blood lipid items, *etc.*) that differed between PNI$^+$ and PNI groups, we used a *t* test. For categorical variables (gender, CA19-9, CEA level and CT-T stage), we utilized χ^2 testing. Multivariate logistic regression was used to examine clinical characteristics with $P < 0.05$ to identify independent clinical predictors. Ultimately, the most effective arterial and venous phase machine learning models were combined with clinically predictive features to create a stacking nomogram. The DeLong test examined whether there were differences

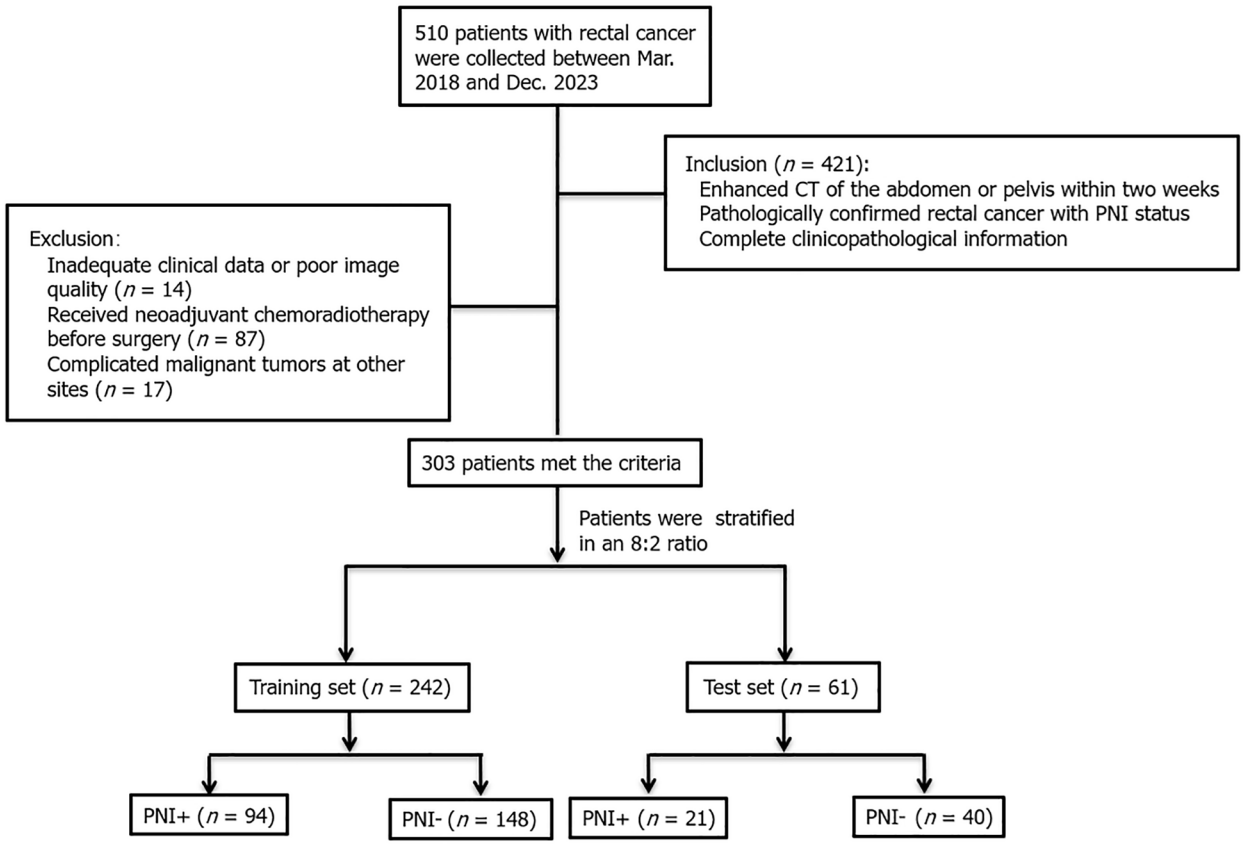

Figure 1 Flow chart of patient recruitment. CT: Computed tomography; PNI: Perineural invasion.

between stacking nomogram, clinical models and the ROC curves of the machine learning models. Hosmer–Lemeshow examined the nomogram for fit, and the model fitted well at $P > 0.05$. The agreement between the actual and anticipated values of the superimposed nomograms was evaluated using calibration curves. The decision curve was employed to evaluate the clinical net-gain of the nomogram.

Statistical analysis

Anaconda (https://www.anaconda.com/python3.7) and R (https://www.r-project.org/version4.1.2) were used for statistical analysis. When comparing the differences between training and test groups for continuous clinical variables, an independent sample *t* test was used if a normal distribution was satisfied; if not, the Mann–Whitney *U* test was utilized to assess the differences. To evaluate the differences between categorical clinical variables, we used Fisher's exact test or χ^2 test. Ultimately, we used multiple logistic regression analysis to identify independent predictors, and two-sided $P < 0.05$ was considered statistically significant.

RESULTS

Clinical features

Age, gender, history of smoking, history of alcohol consumption, CA19-9 level, CEA level, routine blood index, and six blood lipid items did not significantly differ between the PNI and PNI$^+$ groups in the training and test datasets ($P > 0.05$). CT T-stage was shown to be significant in the training and test datasets ($P < 0.05$). Clinical characteristics of the patients are shown in Table 1.

Feature selection

We extracted 3254 radiomic features from each ROI during the arterial and venous phases. Intraclass CC < 0.75 excluded 83 arterial phase features and 94 venous phase features. Then, 131 and 154 features were selected using the Mann–Whitney *U* test. The top 50 features were retained by mRMR, and the last 15 arterial phase and 13 venous phase predictive features were determined by LASSO regression combined with cross-validation.

Construction of the machine learning model

Figure 3 and Table 2 show the ROC curves and AUCs for the four machine learning models. The established radiomics model accurately predicted the preoperative PNI status in RC patients, according to the AUCs of the four machine

Table 2 Performance of four machine learning classifiers (support vector machine, multi-layer perceptron, k-nearest neighbor and logistic regression)

Classifiers	Training set				Test set			
	AUC	95%CI	Sensitivity	Specificity	AUC	95%CI	Sensitivity	Specificity
ASVM	0.904	0.865-0.943	0.840	0.885	0.890	0.794-0.987	0.857	0.850
AKNN	0.790	0.736-0.844	0.638	0.791	0.762	0.640-0.884	0.667	0.725
AMLP	0.821	0.769-0.873	0.840	0.649	0.814	0.691-0.937	0.810	0.750
ALR	0.788	0.731-0.846	0.723	0.730	0.750	0.607-0.893	0.714	0.750
VSVM	0.890	0.850-0.930	0.926	0.703	0.867	0.778-0.956	0.810	0.800
VKNN	0.834	0.783-0.884	0.702	0.838	0.790	0.676-0.904	0.667	0.800
VMLP	0.800	0.744-0.856	0.766	0.730	0.769	0.648-0.890	0.571	0.850
VLR	0.760	0.698-0.822	0.628	0.777	0.735	0.606-0.863	0.999	0.375

ASVM: Arterial support vector machine; AKNN: Arterial k-nearest neighbor; AMLP: Arterial multilayer perceptron; ALR: Arterial logistic regression; VSVM: Venous support vector machine; VKNN: Venous k-nearest neighbor; VMLP: Venous multilayer perceptron; VLR: Venous logistic regression.

learning models. The results showed that arterial SVM (ASVM) and venous SVM (VSVM) had AUCs of 0.904 and 0.890 in the training set, sensitivity of 0.840 and 0.926, and specificity of 0.885 and 0.703, respectively. SVM was the most effective model for the venous and arterial phases. In the test set, the AUC, sensitivity, and specificity of ASVM and VSVM were 0.890 and 0.867, 0.857 and 0.810, and 0.850 and 0.800, respectively. In the training group, the SVM models significantly outperformed the KNN, LR, and MLP models ($P < 0.05$). In the test group, however, the difference between the AUC of the ASVM model and the MLP model was not significant ($P = 0.05938$), nor was the difference between the AUC of the VSVM model and the KNN model ($P = 0.15586$).

Development and validation of the stacking nomogram

The possibility of the SVM model correctly predicting PNI$^+$ during the venous and arterial phases was noted as Arterial_signature and Venous_signature, respectively. Arterial_signature, Venous_signature, and CT-T stage were merged, and logistic regression was used to create the stacking nomogram (Figure 4). With an AUC of 0.964 (95%CI: 0.944-0.983) in the training group and 0.955 (0.900-0.999) in the test group, the stacking nomogram demonstrated a satisfactory evaluation. In the training group, there were significant differences between the ROC curves of the stacking nomogram and the machine learning models in the arterial and venous phases ($P < 0.001$); however, there was no significant difference between the stacking nomogram and the ASVM in the test cohort ($P = 0.05137$). Figure 5 and Tables 3 and 4 show evaluation and comparison of the stacking nomogram, ASVM, VSVM, and CT-T stage. Hosmer–Lemeshow test showed that the stacking nomogram had a good fit (training group: $P = 0.867$, test group: $P = 0.256$). The calibration curve of the stacking nomogram is shown in Figure 5, which illustrates that there is good agreement between the predicted and actual values. A strong net benefit is displayed by the decision curve. Figure 6 shows the radiomics model, clinical model, and stacking nomogram decision curve analysis. The decision curve indicated that, if the threshold likelihood of PNI was between 10% and 90%, the stacking nomogram gained more from treating all patient alternatives or from having no treatment options.

DISCUSSION

According to recent research, PNI is the result of interactions between tumor and nerve cells as well as different biological signaling chemicals and their receptors inside the peripheral milieu. These interactions may cause the cancer to become more aggressive and to spread[13]. Currently, pathological investigation is the sole method available to ascertain PNI status. Preoperative prediction of PNI facilitates the development of individualized treatment. For instance, postoperative chemotherapy and neoadjuvant chemoradiotherapy can help the majority of PNI$^+$ patients, increasing the survival rate [14-16]. Therefore, accurate preoperative prediction of PNI status helps to evaluate the prognosis of RC patients.

The evaluation of noninvasive prognosis in RC patients has always been a difficult issue. Traditional imaging methods, such as CT and MRI, cannot accurately predict the PNI status of RC; however, RC is a temporally and spatially heterogeneous disease. The risk of invasive sampling and potential complications limit its application in tumor progression and real-time monitoring, so radiomics gradually attracted the attention of oncologists and clinicians. There have been several studies using radiomics to assess PNI status in RC. Chen *et al*[17] proposed a nomogram model for predicting preoperative PNI status in colorectal cancer (training group, AUC = 0.88; test group, AUC = 0.80), including radiomics features, CT-T stage and CT-N stage levels. Yang *et al*[18] predicted the preoperative PNI nomogram based on MRI, including radiomics characteristics, MRI-T stage (training group, AUC = 0.81; test group, AUC = 0.75). In this study, we developed and validated a PNI for CT preoperatively (training group, AUC = 0.964; test group, AUC = 0.955). Our results

Table 3 Prediction performance of four models (arterial support vector machine, venous support vector machine, CT-Tstage and Nomogram)

Model	Dataset	AUC	95%CI	Sensitivity	Specificity	Recall	Accuracy	Precision	F1-score
ASVM	Train	0.904	0.865-0.943	0.840	0.885	0.840	0.863	0.880	0.860
	Test	0.890	0.794-0.987	0.857	0.850	0.857	0.854	0.851	0.854
VSVM	Train	0.890	0.850-0.930	0.926	0.703	0.926	0.815	0.757	0.786
	Test	0.867	0.778-0.956	0.810	0.800	0.810	0.805	0.802	0.806
CT-Tstage	Train	0.647	0.583-0.710	0.553	0.689	0.553	0.621	0.640	0.593
	Test	0.730	0.607-0.854	0.525	0.825	0.525	0.675	0.750	0.618
Nomogram	Train	0.964	0.944-0.983	0.800	0.789	0.800	0.795	0.791	0.795
	Test	0.955	0.900-0.999	0.952	0.900	0.952	0.928	0.905	0.919

AUC: Area under curve; ASVM: Arterial support vector machine; VSVM: Venous support vector machine.

Table 4 Delong-test results of four models (Arterial support vector machine, venous support vector machine, CT-T stage and Nomogram)

Model	Training set				Test set			
Delong-test	ASVM	VSVM	CT-T stage	Nomogram	ASVM	VSVM	CT-T stage	Nomogram
ASVM	-	0.6304	**1.934e-11**	**0.000271**	-	0.6997	0.0527	0.05137
VSVM	-	-	**1.737e-10**	**2.15e-05**	-	-	0.0692	**0.03611**
CT-Tstage	-	-	-	**2.2e-16**	-	-	-	**0.000305**
Nomogram	-	-	-	-	-	-	-	-

ASVM: Arterial support vector machine; VSVM: Venous support vector machine; $P < 0.05$.

showed that the CT deep learning-radiomics stacking nomogram can identify the PNI status of RC before surgery, provide a quantitative, efficient, and noninvasive mechanism for PNI status identification in RC patients, and guide personalized treatment. In this study, T stage as assessed by CT was an independent clinical predictor of PNI, suggesting that tumor invasive depth was significantly associated with PNI. With increased T stage, increased proliferation and aggressiveness of tumor cells, and increased risk of PNI in colorectal cancer patients, which is consistent with previous studies[17-19]. Histopathological predictors from surgical pathological tissue may lead to sampling bias; therefore, we combined radiomics characteristics and clinical risk factors based on arterial and venous enhanced CT into an easy-to-use nomogram to facilitate noninvasive individualized prediction of PNI status in RC patients and to determine treatment strategies.

To construct the radiomics model, we screened 15 and 13 radiomics features highly associated with PNI from the arterial and venous stages, respectively. In both arterial and venous stages, the radiomics features GLSZM-small area emphasis showed a negative correlation with PNI of RC. GLSZM is defined as the number of connecting elements with the same gray intensity. Small area emphasis is a measure of regional distribution of small size, with larger values representing smaller areas and better texture, which indicates that PNI-positive tumors have rough texture features, and more detailed features are needed to describe PNI-negative tumors. These reflect the existence of some specific connection between tumor intensity, differences within tumor texture, and PNI. Previous studies also showed that texture features are predictive in many cases, which is consistent with the results of this study[19,20].

A large number of studies on disease classification, differential diagnosis and predictive prognosis have shown that deep learning can better promote radiomics analysis, which is becoming more widely used in the field of medical imaging. The use of deep learning methods to process and analyze medical imaging data has promoted the development of precision and personalized medicine[21,22]. Deep learning features comprised most of the features that we screened (25 of 28), suggesting that deep learning is more predictively significant in the preoperative PNI prediction of RC. We constructed a neural network by transfer learning using the Resnet-50 method to provide machine learning models with strong feature representation capabilities. Transfer learning is a generalized and efficient method of learning that involves applying knowledge from tasks related to general object recognition to challenges specific to a certain domain. Therefore, the main contribution of this study is to use the ImageNet pretrained deep learning CNN architecture as the foundation to establish an automated tool for the detection and diagnosis of PNI in CT images. Its main idea is to use their CNN structure and its learning weights on ImageNet, and use the ResNet50 architecture to accurately extract features from the ROIs. The Resnet-50 algorithm is based on the residual learning mechanism. The algorithm simplifies the learning

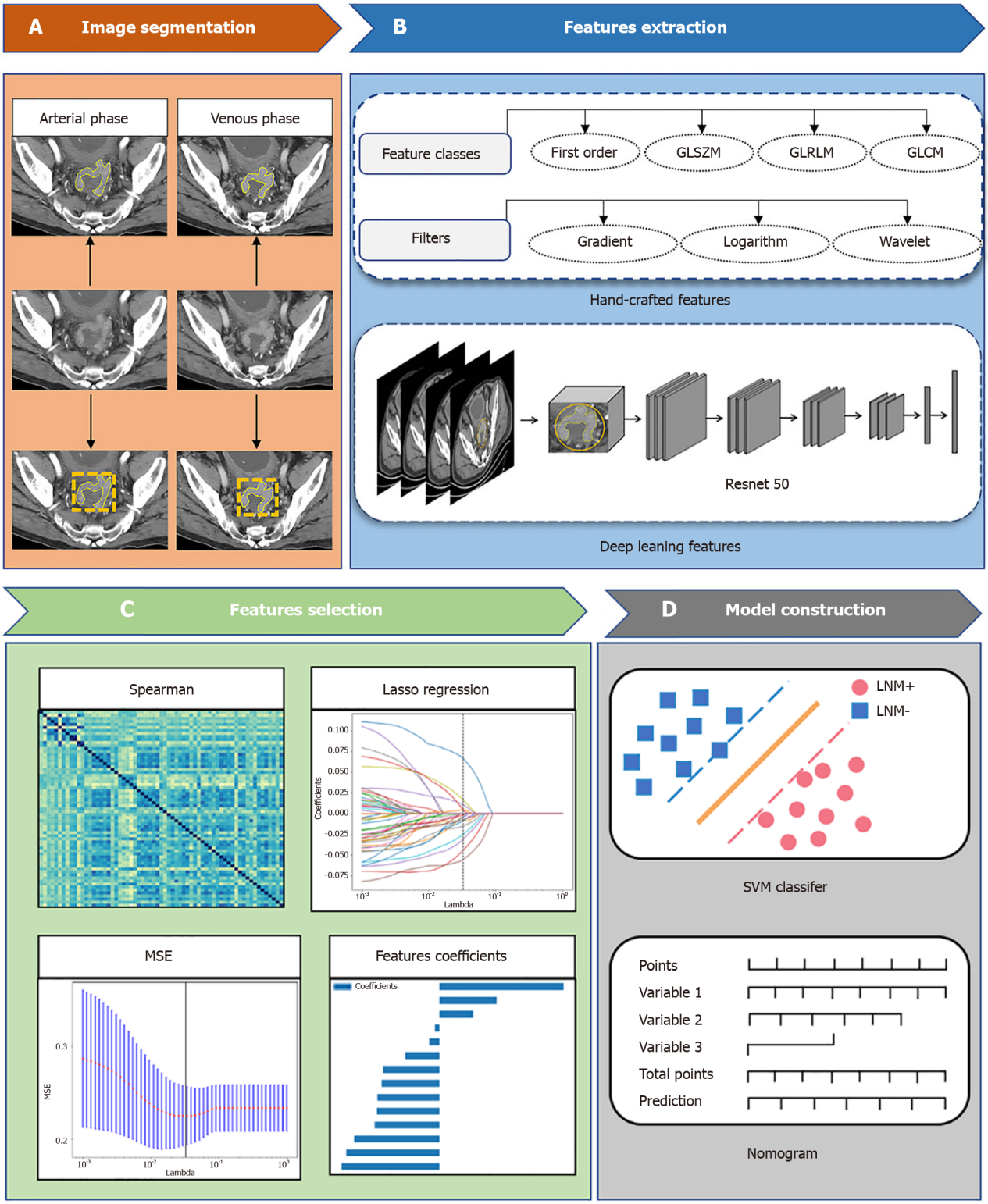

Figure 2 Demonstration of radiomics model construction. A: Image segmentation; B: Features extraction; C: Features selection; D: Model construction.

process, making it possible to train deeper networks, and solves the problem of gradient dispersion and disappearance as the network deepens. Research has demonstrated that a range of tumor-related tasks, such as tumor diagnosis, classification, grade, stage, and prognostic prediction, as well as identification of pathological features, biomarkers, and genetic alterations, may be carried out using CNN algorithms based on Resnet50. Several studies have also demonstrated the clinical utility of this architecture of Resnet-50[23-25].

Selecting the right machine learning model is essential for maintaining the stability and performance of the model. Many researchers[18,20] only used one machine learning technique to create their models. Chen *et al*[20] discovered that the logistic-regression-based MR radiomics model was effective in predicting PNI in patients with colorectal cancer (AUC = 0.86 in the training group; AUC = 0.85 in the test group). This study investigated the diagnostic performance of four machine learning models built on the KNN, SVM, MLP, and LR machine learning algorithms. With AUC values greater

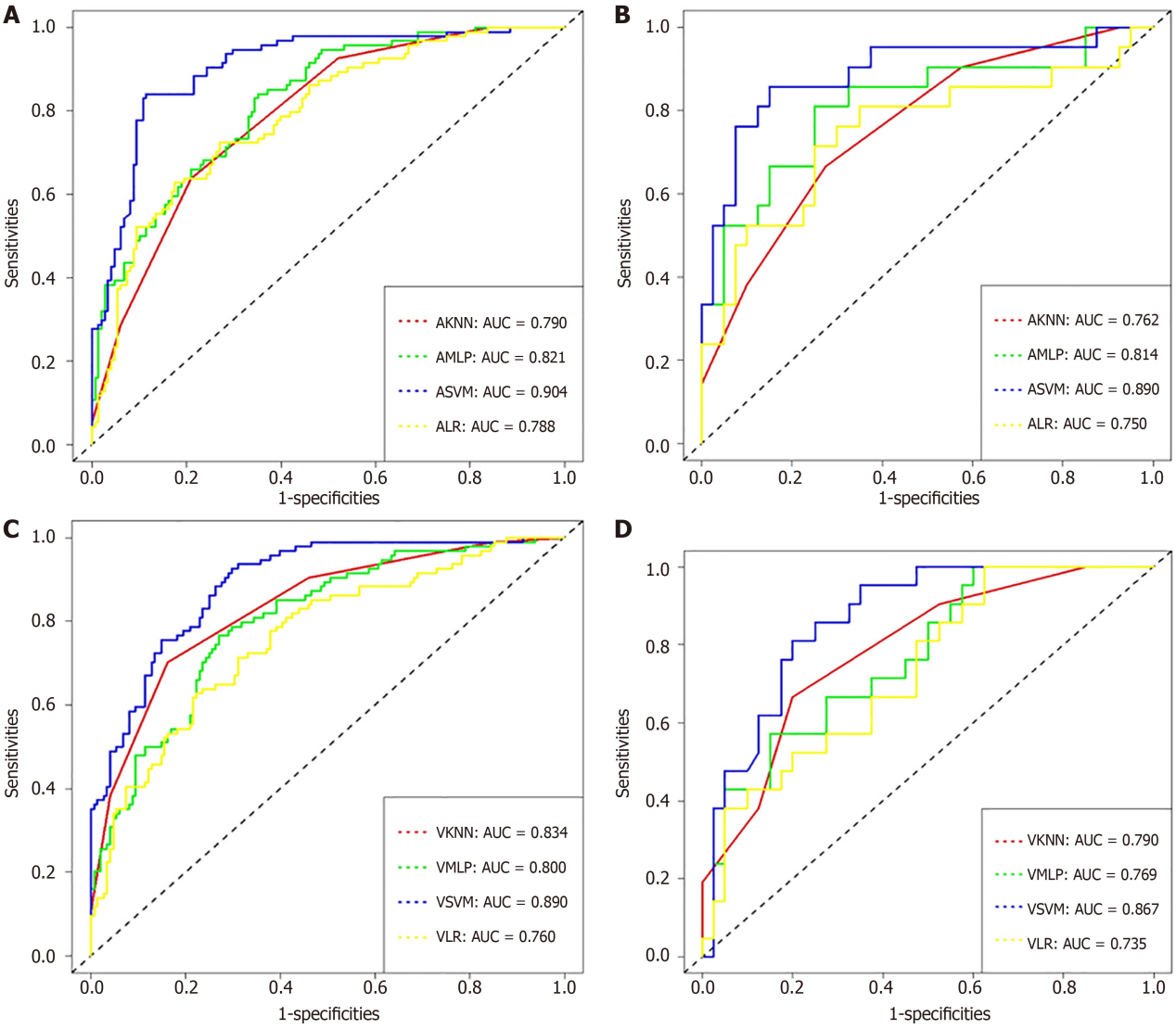

Figure 3 Receiver operating characteristic curves of the support vector machine, multi-layer perceptron, k-nearest neighbor and logistic regression. A: Receiver operating characteristic (ROC) curves of arterial support vector machine (ASVM), arterial multilayer perceptron (AMLP), arterial k-nearest neighbor (AKNN) and arterial logistic regression (ALR) in the Training set; B: ROC curves of ASVM, AMLP, AKNN and ALR in the test set; C: ROC curves of VSVM, VMLP, VKNN and VLR in the Training set; D: ROC curves of VSVM, VMLP, VKNN and VLR in the test set.

than KNN, MLP, and LR algorithms (training group: AUC = 0.904; validation group: AUC = 0.890), SVM was the best machine learning method. In the realm of machine learning, SVMs are examples of classical classification algorithms. The SVM is known as the most robust classifier and has good generalization ability, suitability for small samples, and high dimensional features. It has been applied extensively to numerous classification and regression issues, yielding positive outcomes[26,27]. To further improve the ability to predict PNI, we constructed a stacking nomogram model using the input variable obtained by the above SVM machine learning algorithm. The AUC of this stacking nomogram model (training group, AUC = 0.964; test group, AUC = 0.955) improved the AUC compared with a single machine learning model and higher than the recently reported results (training group, AUC = 0.88; test group, AUC = 0.80) [17]. Although the increase in AUC of the stacking nomogram model was not significant compared with the machine learning ASVM model (P = 0.051), this may be due to the small sample size of the test set in this study, which cannot reflect the significance of the intermodel differences.

Our study had some limitations. This was a retrospective study conducted in a single center, hence adequate external data are required to validate the findings. Our sample size was small, and future research and data from other centers are required to confirm the generalizability of our model. These could be useful directions for future investigation.

CONCLUSION

We provide a stacking nomogram model of radiomics based on contrast-enhanced CT that may predict the PNI status of RC and provide clinicians with additional quantifiable evidence for the formulation of individualized treatment options.

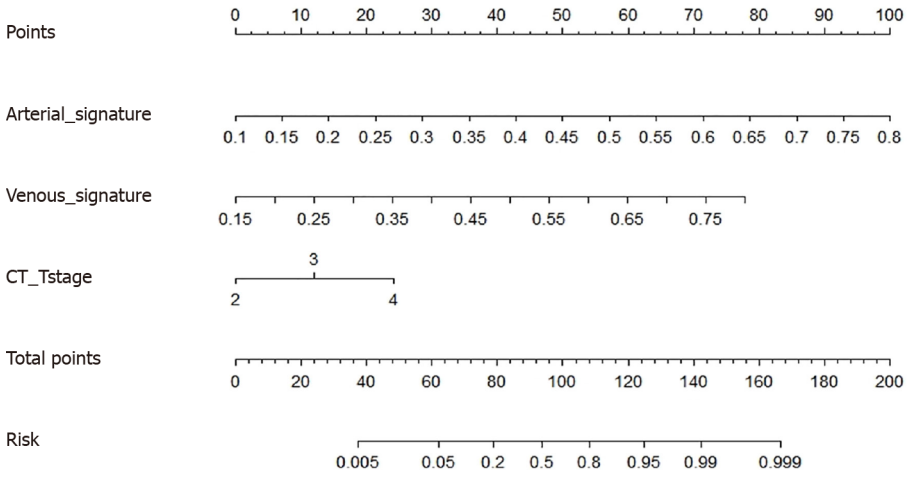

Figure 4 Nomogram based on the radiomics feature and clinical predictors.

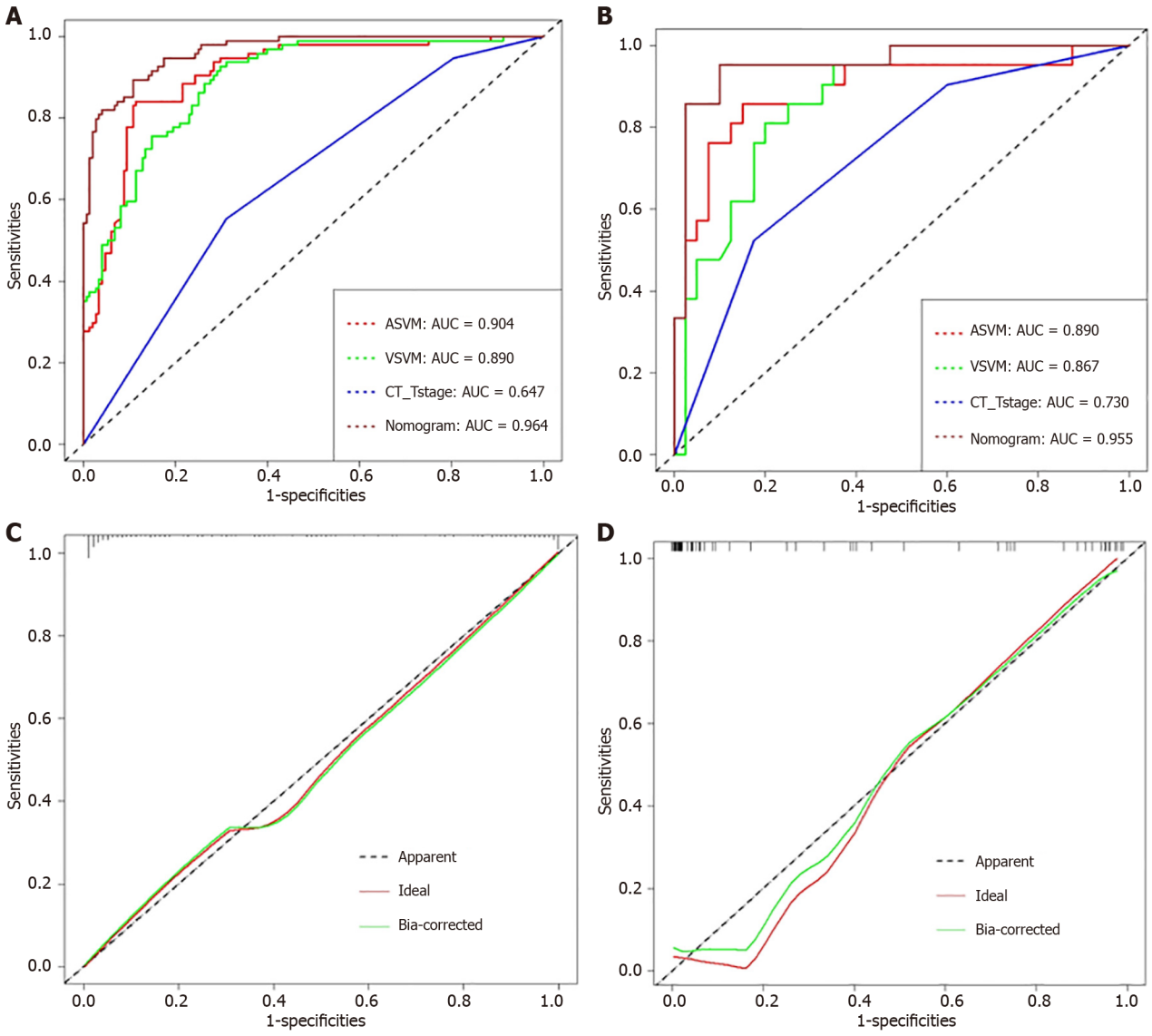

Figure 5 Receiver operating characteristic curves and calibration curves for training and test set. A: Receiver operating characteristic (ROC) curves of CT_Tstage, arterial support vector machine (ASVM), enous support vector machine (VSVM) and stacking nomogram in the Training set; B: ROC curves of CT_Tstage, ASVM, VSVM and stacking nomogram in the Test set; C: Calibration curves of the stacking nomograms in the training set; D: Calibration curves of the stacking nomograms in the test set. X-axis represents the predicted risk of perineural invasion (PNI). Y-axis represents the actual PNI.

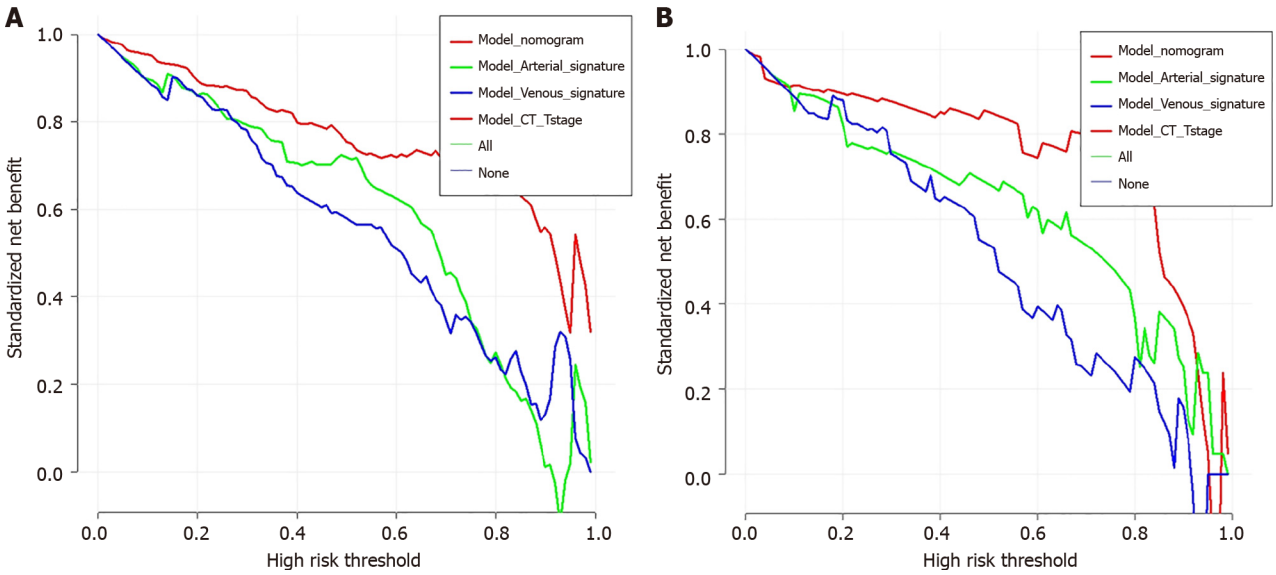

Figure 6 Decision curve analysis of four model. A: Decision curve analysis of four model in the training set; B: Decision curve analysis of four model in the test set.

ACKNOWLEDGEMENTS

Thanks to the Fourth Affiliated Hospital of China Medical University for technical support of this study.

FOOTNOTES

Author contributions: Zhao ZC and Liu JX contributed to data curation and analysis; Liu JX contributed to methodology, conceptualization, writing (original draft), and validation; Sun LL contributed to supervision and resources; all authors contributed to the study conception and design; all authors have read and approved the final manuscript.

Institutional review board statement: This retrospective study was approved by the medical ethics committee of our hospital (Ethical review number: EC-2022-KS-035).

Informed consent statement: The need for informed consent from all individual participants included in study was waived.

Conflict-of-interest statement: The authors of this manuscript declare no relationships with any companies whose products or services may be related to the subject matter of this article.

Data sharing statement: Dataset available from the corresponding author at 3304352470@qq.com.

Country of origin: China

ORCID number: Jia-Xuan Liu 0009-0002-9838-1384.

S-Editor: Liu JH
L-Editor: A
P-Editor: Yu HG

REFERENCES

1 **Siegel RL**, Miller KD, Fuchs HE, Jemal A. Cancer statistics, 2022. *CA Cancer J Clin* 2022; **72**: 7-33 [PMID: 35020204 DOI: 10.3322/caac.21708]

2 **Liu Q**, Ma Z, Cao Q, Zhao H, Guo Y, Liu T, Li J. Perineural invasion-associated biomarkers for tumor development. *Biomed Pharmacother* 2022; **155**: 113691 [PMID: 36095958 DOI: 10.1016/j.biopha.2022.113691]

3 **Fu Y**, Zhang X, Ding Z, Zhu N, Song Y, Zhang X, Jing Y, Yu Y, Huang X, Zhang L, Hu Q, Ni Y, Ding L. Worst Pattern of Perineural Invasion Redefines the Spatial Localization of Nerves in Oral Squamous Cell Carcinoma. *Front Oncol* 2021; **11**: 766902 [PMID: 34912713 DOI: 10.3389/fonc.2021.766902]

4 **Kaya T**, Dursun A. Can Lymphovascular and Perineural Invasion be Additional Staging Criteria in Colorectal Cancer? *J Coll Physicians Surg Pak* 2021; **31**: 657-662 [PMID: 34102776 DOI: 10.29271/jcpsp.2021.06.657]

5 **Li M**, Jin YM, Zhang YC, Zhao YL, Huang CC, Liu SM, Song B. Radiomics for predicting perineural invasion status in rectal cancer. *World J Gastroenterol* 2021; **27**: 5610-5621 [PMID: 34588755 DOI: 10.3748/wjg.v27.i33.5610]

6 **Kim S**, Huh JW, Lee WY, Yun SH, Kim HC, Cho YB, Park YA, Shin JK. Prognostic Impact of Lymphatic Invasion, Venous Invasion, Perineural Invasion, and Tumor Budding in Rectal Cancer Treated With Neoadjuvant Chemoradiotherapy Followed by Total Mesorectal Excision. *Dis Colon Rectum* 2023; **66**: 905-913 [PMID: 35195558 DOI: 10.1097/DCR.0000000000002266]

7 **Lafata KJ**, Wang Y, Konkel B, Yin FF, Bashir MR. Radiomics: a primer on high-throughput image phenotyping. *Abdom Radiol (NY)* 2022; **47**: 2986-3002 [PMID: 34435228 DOI: 10.1007/s00261-021-03254-x]

8 **Mayerhoefer ME**, Materka A, Langs G, Häggström I, Szczypiński P, Gibbs P, Cook G. Introduction to Radiomics. *J Nucl Med* 2020; **61**: 488-495 [PMID: 32060219 DOI: 10.2967/jnumed.118.222893]

9 **Bera K**, Braman N, Gupta A, Velcheti V, Madabhushi A. Predicting cancer outcomes with radiomics and artificial intelligence in radiology. *Nat Rev Clin Oncol* 2022; **19**: 132-146 [PMID: 34663898 DOI: 10.1038/s41571-021-00560-7]

10 **Guo Y**, Wang Q, Guo Y, Zhang Y, Fu Y, Zhang H. Preoperative prediction of perineural invasion with multi-modality radiomics in rectal cancer. *Sci Rep* 2021; **11**: 9429 [PMID: 33941817 DOI: 10.1038/s41598-021-88831-2]

11 **Ma J**, Guo D, Miao W, Wang Y, Yan L, Wu F, Zhang C, Zhang R, Zuo P, Yang G, Wang Z. The value of (18)F-FDG PET/CT-based radiomics in predicting perineural invasion and outcome in non-metastatic colorectal cancer. *Abdom Radiol (NY)* 2022; **47**: 1244-1254 [PMID: 35218381 DOI: 10.1007/s00261-022-03453-0]

12 **Cerminara SE**, Cheng P, Kostner L, Huber S, Kunz M, Maul JT, Böhm JS, Dettwiler CF, Geser A, Jakopović C, Stoffel LM, Peter JK, Levesque M, Navarini AA, Maul LV. Diagnostic performance of augmented intelligence with 2D and 3D total body photography and convolutional neural networks in a high-risk population for melanoma under real-world conditions: A new era of skin cancer screening? *Eur J Cancer* 2023; **190**: 112954 [PMID: 37453242 DOI: 10.1016/j.ejca.2023.112954]

13 **Chen SH**, Zhang BY, Zhou B, Zhu CZ, Sun LQ, Feng YJ. Perineural invasion of cancer: a complex crosstalk between cells and molecules in the perineural niche. *Am J Cancer Res* 2019; **9**: 1-21 [PMID: 30755808]

14 **Kim S**, Huh JW, Lee WY, Yun SH, Kim HC, Cho YB, Park YA, Shin JK. Lymphovascular invasion, perineural invasion, and tumor budding are prognostic factors for stage I colon cancer recurrence. *Int J Colorectal Dis* 2020; **35**: 881-885 [PMID: 32112198 DOI: 10.1007/s00384-020-03548-4]

15 **Sung SY**, Kim SH, Jang HS, Song JH, Jeong S, Jung JH, Lee JH. Pathologic Implications of Radial Resection Margin and Perineural Invasion to Adjuvant Chemotherapy after Preoperative Chemoradiotherapy and Surgery for Rectal Cancer: A Multi-Institutional and Case-Matched Control Study. *Cancers (Basel)* 2022; **14** [PMID: 36077649 DOI: 10.3390/cancers14174112]

16 **Kim CH**, Yeom SS, Lee SY, Kim HR, Kim YJ, Lee KH, Lee JH. Prognostic Impact of Perineural Invasion in Rectal Cancer After Neoadjuvant Chemoradiotherapy. *World J Surg* 2019; **43**: 260-272 [PMID: 30151676 DOI: 10.1007/s00268-018-4774-8]

17 **Chen Q**, Cui Y, Xue T, Peng H, Li M, Zhu X, Duan S, Gu H, Feng F. Computed tomography-based radiomics nomogram for the preoperative prediction of perineural invasion in colorectal cancer: a multicentre study. *Abdom Radiol (NY)* 2022; **47**: 3251-3263 [PMID: 35960308 DOI: 10.1007/s00261-022-03620-3]

18 **Yang YS**, Qiu YJ, Zheng GH, Gong HP, Ge YQ, Zhang YF, Feng F, Wang YT. High resolution MRI-based radiomic nomogram in predicting perineural invasion in rectal cancer. *Cancer Imaging* 2021; **21**: 40 [PMID: 34039436 DOI: 10.1186/s40644-021-00408-4]

19 **Zhang Y**, Peng J, Liu J, Ma Y, Shu Z. Preoperative Prediction of Perineural Invasion Status of Rectal Cancer Based on Radiomics Nomogram of Multiparametric Magnetic Resonance Imaging. *Front Oncol* 2022; **12**: 828904 [PMID: 35480114 DOI: 10.3389/fonc.2022.828904]

20 **Chen J**, Chen Y, Zheng D, Pang P, Zhang H, Zheng X, Liao J. Pretreatment MR-based radiomics nomogram as potential imaging biomarker for individualized assessment of perineural invasion status in rectal cancer. *Abdom Radiol (NY)* 2021; **46**: 847-857 [PMID: 32870349 DOI: 10.1007/s00261-020-02710-4]

21 **Bo L**, Zhang Z, Jiang Z, Yang C, Huang P, Chen T, Wang Y, Yu G, Tan X, Cheng Q, Li D, Liu Z. Differentiation of Brain Abscess From Cystic Glioma Using Conventional MRI Based on Deep Transfer Learning Features and Hand-Crafted Radiomics Features. *Front Med (Lausanne)* 2021; **8**: 748144 [PMID: 34869438 DOI: 10.3389/fmed.2021.748144]

22 **Wang H**, Wang L, Lee EH, Zheng J, Zhang W, Halabi S, Liu C, Deng K, Song J, Yeom KW. Decoding COVID-19 pneumonia: comparison of deep learning and radiomics CT image signatures. *Eur J Nucl Med Mol Imaging* 2021; **48**: 1478-1486 [PMID: 33094432 DOI: 10.1007/s00259-020-05075-4]

23 **Elpeltagy M**, Sallam H. Automatic prediction of COVID- 19 from chest images using modified ResNet50. *Multimed Tools Appl* 2021; **80**: 26451-26463 [PMID: 33967592 DOI: 10.1007/s11042-021-10783-6]

24 **Sharma AK**, Nandal A, Dhaka A, Koundal D, Bogatinoska DC, Alyami H. Enhanced Watershed Segmentation Algorithm-Based Modified ResNet50 Model for Brain Tumor Detection. *Biomed Res Int* 2022; **2022**: 7348344 [PMID: 35252454 DOI: 10.1155/2022/7348344]

25 **Hossain MB**, Iqbal SMHS, Islam MM, Akhtar MN, Sarker IH. Transfer learning with fine-tuned deep CNN ResNet50 model for classifying COVID-19 from chest X-ray images. *Inform Med Unlocked* 2022; **30**: 100916 [PMID: 35342787 DOI: 10.1016/j.imu.2022.100916]

26 **Dong D**, Fang MJ, Tang L, Shan XH, Gao JB, Giganti F, Wang RP, Chen X, Wang XX, Palumbo D, Fu J, Li WC, Li J, Zhong LZ, De Cobelli F, Ji JF, Liu ZY, Tian J. Deep learning radiomic nomogram can predict the number of lymph node metastasis in locally advanced gastric cancer: an international multicenter study. *Ann Oncol* 2020; **31**: 912-920 [PMID: 32304748 DOI: 10.1016/j.annonc.2020.04.003]

27 **Aswathy MA**, Jagannath M. An SVM approach towards breast cancer classification from H&E-stained histopathology images based on integrated features. *Med Biol Eng Comput* 2021; **59**: 1773-1783 [PMID: 34302269 DOI: 10.1007/s11517-021-02403-0]

Artificial Intelligence in Medical Imaging

Submit a Manuscript: https://www.f6publishing.com

Artif Intell Med Imaging 2024 September 28; 5(1): 97356

DOI: 10.35711/aimi.v5.i1.97356

ISSN 2644-3260 (online)

LETTER TO THE EDITOR

Criteria for assessing the diagnostic significance of modern methods of imaging gastrointestinal diseases in practical gastroenterology

Sergey M Kotelevets

Specialty type: Oncology

Provenance and peer review: Invited article; Externally peer reviewed.

Peer-review model: Single-blind

Peer-review report's classification

Scientific Quality: Grade B

Novelty: Grade B

Creativity or Innovation: Grade C

Scientific Significance: Grade C

P-Reviewer: Goel A

Received: May 28, 2024

Revised: August 29, 2024

Accepted: September 10, 2024

Published online: September 28, 2024

Processing time: 120 Days and 17.5 Hours

Sergey M Kotelevets, Department of Therapy, Medical Institute, North Caucasus State Academy, Cherkessk 369000, Russia

Corresponding author: Sergey M Kotelevets, MD, Professor, Department of Therapy, Medical Institute, North Caucasus State Academy, Stavropolskaya Street 36, Cherkessk 369000, Russia. smkotelevets@mail.ru

Abstract

Imaging methods are frequently used to diagnose gastrointestinal diseases and play a crucial role in verifying clinical diagnoses among all diagnostic algorithms. However, these methods have limitations, challenges, benefits, and advantages. Addressing these limitations requires the application of objective criteria to assess the effectiveness of each diagnostic method. The diagnostic process is dynamic and requires a consistent algorithm, progressing from clinical subjective data, such as patient history (anamnesis), and objective findings to diagnostics *ex juvantibus*. Caution must be exercised when interpreting diagnostic results, and there is an urgent need for better diagnostic tests. In the absence of such tests, preliminary criteria and a diagnosis *ex juvantibus* must be relied upon. Diagnostic imaging methods are critical stages in the diagnostic workflow, with sensitivity, specificity, and accuracy serving as the primary criteria for evaluating clinical, laboratory, and instrumental symptoms. A comprehensive evaluation of all available diagnostic data guarantees an accurate diagnosis. The "gold standard" for diagnosis is typically established through either the results of a pathological autopsy or a lifetime diagnosis resulting from a thorough examination using all diagnostic methods.

Key Words: Imaging methods; Gastrointestinal diseases; Sensitivity; Specificity; Accuracy of the method

Core Tip: The diagnostic process is a complex journey that every physician undertakes with each patient. Successfully diagnosing gastrointestinal diseases requires mastery of all the methods within the diagnostic algorithm. Modern imaging methods provide physicians with significant diagnostic support. But how should the results of these imaging methods be evaluated? This is done using key criteria such as sensitivity, specificity, and accuracy. Only a comprehensive assessment of various diagnostic methods, taking into account these criteria, will ensure the correct diagnosis of the disease.

Citation: Kotelevets SM. Criteria for assessing the diagnostic significance of modern methods of imaging gastrointestinal diseases in practical gastroenterology. *Artif Intell Med Imaging* 2024; 5(1): 97356
URL: https://www.wjgnet.com/2644-3260/full/v5/i1/97356.htm
DOI: https://dx.doi.org/10.35711/aimi.v5.i1.97356

TO THE EDITOR

Imaging methods are frequently used to diagnose gastrointestinal diseases, serving as crucial tools to verify clinical diagnoses across various diagnostic algorithms (Table 1). These methods, however, have their limitations, challenges, benefits, and advantages. To address these limitations, it is necessary to apply objective criteria to evaluate the effectiveness of each diagnostic method. Non-invasive imaging techniques, such as ultrasound, CT, positron emission tomography (PET), and MRI, have revolutionized gastrointestinal diagnostics over the past few decades. Advancements in imaging resolution, three-dimensional imaging, and contrast agents have significantly improved diagnostic accuracy. Studies indicate remarkable diagnostic accuracy for various bowel conditions. For instance, inflammatory bowel diseases can be detected with 73%-87% sensitivity, while ulcerative colitis can be detected with 89% sensitivity and 100% specificity. Ultrasound also shows strong performance in diagnosing acute appendicitis (80%-93% sensitivity and 94%-100% specificity) and acute colonic diverticulitis (84%-100% sensitivity), achieving diagnostic accuracy comparable to that of CT scans[1]. In addition, literature reviews on the diagnosis of Crohn's disease and its complications using small intestine contrast ultrasonography report sensitivity and specificity rates of 88% and 86%, respectively, for detecting small bowel lesions[2-4]. Assessing intestinal wall thickness further enhances the accuracy of this diagnostic method, with sensitivity, specificity, and accuracy values of 98%, 100%, and 98.3%, respectively[5]. Comparative studies reveal satisfactory performance for endoscopic studies and contrast-enhanced magnetic resonance (MR) enterography. Endoscopy has a sensitivity of 81.3% and a specificity of 70.5%, while MR enterography has a sensitivity of 80.2% and a specificity of 84.0%[6]. The diagnostic accuracy of imaging largely depends on the skill and expertise of the diagnostician. To ensure accurate interpretation and reduce diagnostic errors, radiologists need to thoroughly understand the factors that contribute to false-positive and false-negative findings[7,8]. To enhance diagnostic precision, optimal protocols tailored to the chosen imaging methods must be employed[9].

IMAGING METHODS FOR DIAGNOSING DIGESTIVE ORGAN NEOPLASMS

Imaging techniques are essential for diagnosing gastrointestinal cancers, although their accuracy varies depending on the type of cancer and the method used. For gastric cancer, fasting whole-body PET/CT scans demonstrate a sensitivity of 92.9% and a specificity of 75%, with a positive predictive value of 94.5% and a negative predictive value of 69%. Enhancing these results by adding a mixture of milk and diatrizoate meglumine increases sensitivity to 91.1%, specificity to 91.7%, positive predictive value to 98.1%, and negative predictive value to 68.8%[10]. However, routine PET/CT scans may not be ideal for the initial staging of diffuse-type gastric cancer or for restaging lymph nodes after neoadjuvant treatment owing to lower sensitivities, which are reported at 24% and 32%, respectively. CT scans are useful in evaluating the primary gastric tumor and detecting liver metastasis, with sensitivity ranging from 54.5% to 72.7% and specificity from 89.3% to 94.6%, depending on the interpreting radiologist. The positive predictive value varies from 57.1% to 66.7%, while the negative predictive value ranges from 91.4% to 94.3%, highlighting the impact of radiologist interpretation on diagnostic accuracy[11,12]. For esophageal squamous cell carcinoma, multidetector CT shows variable diagnostic efficiency, with sensitivity ranging from 62.5% to 96.9%, specificity from 77.9% to 98.5%, and overall accuracy from 73% to 98%. The effectiveness of multidetector CT depends on the assessment criteria used, such as measuring the maximum esophageal wall thickness (≤ 9 mm) or the average attenuation of the esophageal wall (≤ 64 HU). These findings emphasize that, while imaging is indispensable for diagnosing and managing gastrointestinal cancers, factors such as the specific technique, the type and stage of cancer, the assessment criteria, and even the interpreting radiologist's experience significantly influence the accuracy and reliability of the results[13]. There are conflicting results regarding the effectiveness of various imaging techniques for diagnosing gastrointestinal tumors[14-16]. However, diagnostic efficiency significantly improves when two modern imaging methods are combined, leading to substantially increased sensitivity, specificity, and accuracy[17-20]. High sensitivity, specificity, and accuracy of diagnostic methods not only enable the detection of disease but also help determine its activity and severity. For example, dual-energy CT enterography can measure iodine density, a criterion that reflects Crohn's disease activity and correlates well with histological analysis[21]. This raises a question regarding the method that can serve as the reference standard when assessing the performance of imaging techniques (radiological or endoscopic diagnostics). Histopathological analysis is often seen as the gold

Table 1 Classification of diagnostic methods

Groups of diagnostic methods	Criteria for assessing the diagnostic effectiveness of a method (symptom)
Clinical methods	Sensitivity, specificity, and accuracy
Subjective symptoms	-
Complaints	-
Anamnesis	-
Objective symptoms	-
Data of objective findings, somatic symptoms	-
Additional methods	-
Laboratory symptoms	-
Biochemical methods	-
Immuno-enzyme methods	-
Immunological methods	-
Molecular genetic methods	-
Bacteriological methods	-
Histopathological and cytological methods	-
Instrumental methods	-
Symptoms of radiation methods	-
Endoscopic symptoms	-
Symptoms of other methods	-
Method ex juvantibus	-

The reference "gold standard" method is typically established through either a pathological autopsy or a lifetime diagnosis obtained from a comprehensive examination that incorporates all available diagnostic methods.

standard, but it has its challenges. Various histopathological methods, such as biopsies in living patients, may yield conflicting results for the same disease in different individuals[22]. Factors influencing the accuracy of diagnostic methods include the technological sophistication of the equipment and the professional expertise of the diagnostician.

IMAGING METHODS FOR DIAGNOSING OTHER DISEASES

Imaging methods have high sensitivity and negative predictive value for diagnosing esophageal perforation. Thoracic CT has proven highly reliable in ruling out esophageal perforation, demonstrating 100% sensitivity and negative predictive value. This means that if the thoracic CT scan appears normal, patients can confidently be cleared of this complication. However, while the test excels at excluding perforation, it is less accurate in confirming its presence. Specifically, although the sensitivity for detecting esophageal perforation is a perfect 100%, ensuring that all perforations are identified, the specificity is lower at 54.6%, suggesting a higher chance of false positives. This is reflected in a positive predictive value of only 23.4%, meaning that only about one in four suspected cases based on the scan are true perforations[23]. For detecting choledocholithiasis, CT with contrast has moderate diagnostic effectiveness, with a sensitivity ranging from 77% to 88%, specificity ranging from 50% to 71%, and overall accuracy ranging from 71% to 74%[24]. MRI shows high diagnostic performance in pediatric appendicitis, with both sensitivity and specificity reaching 97%. Receiver operating characteristic analysis revealed an area under the curve of 0.98, indicating a high level of accuracy[25].

Diagnosing intestinal ischemia using clinical and laboratory methods is challenging. However, modern imaging methods offer improved diagnostic accuracy. For the first experienced radiologist, sensitivity, specificity, positive predictive value, negative predictive value, and accuracy were 62.0%, 87.5%, 88.6%, 59.6%, and 72.0%, respectively, and for the second experienced radiologist, the corresponding values were 58.0%, 93.8%, 93.5%, 58.8%, and 72.0%[26]. To enhance the effectiveness of instrumental diagnostics, it is recommended to combine different imaging techniques and use multiple diagnostic approaches in conjunction.

CONCLUSION

The diagnostic process is dynamic and requires a consistent algorithm of diagnostic methods, from clinical subjective data (anamnesis) and objective findings to diagnostics ex juvantibus. Current diagnostic methods for these conditions are recognized as imperfect, necessitating caution in their application and underscoring the urgent need for more reliable diagnostic tools. Until such tools become available, clinicians must depend on preliminary criteria and diagnoses based on a patient's response to treatment, which is inherently less reliable than a definitive diagnostic test[27,28]. Diagnostic imaging methods play a crucial role in this process. Sensitivity, specificity, and accuracy are key indicators used to evaluate the effectiveness of diagnostic methods across all diagnostic symptoms (clinical, laboratory, and instrumental). To avoid diagnostic errors, it is necessary to combine various instrumental diagnostic methods. The diagnostician must be highly trained, and it is recommended that two diagnosticians assess each imaging method. A comprehensive evaluation of all available diagnostic symptoms guarantees a correct diagnosis.

FOOTNOTES

Author contributions: Kotelevets SM contributed to this paper by designing the overall concept, outlining the manuscript, drafting its content, writing and editing, creating illustrations, reviewing relevant literature, and approving the final version for publication.

Conflict-of-interest statement: The author, Sergey M Kotelevets, has nothing to disclose.

Country of origin: Russia

ORCID number: Sergey M Kotelevets 0000-0003-4915-6869.

S-Editor: Luo ML
L-Editor: Filipodia
P-Editor: Yu HG

REFERENCES

1 **Roccarina D**, Garcovich M, Ainora ME, Caracciolo G, Ponziani F, Gasbarrini A, Zocco MA. Diagnosis of bowel diseases: the role of imaging and ultrasonography. *World J Gastroenterol* 2013; **19**: 2144-2153 [PMID: 23599640 DOI: 10.3748/wjg.v19.i14.2144]

2 **Zhu C**, Ma X, Xue L, Xu J, Li Q, Wang Y, Zhang J. Small intestine contrast ultrasonography for the detection and assessment of Crohn disease: A meta-analysis. *Medicine (Baltimore)* 2016; **95**: e4235 [PMID: 27495028 DOI: 10.1097/MD.0000000000004235]

3 **Ponorac S**, Gošnak RD, Urlep D, Ključevšek D. Contrast-enhanced ultrasonography in the evaluation of Crohn disease activity in children: comparison with histopathology. *Pediatr Radiol* 2021; **51**: 410-418 [PMID: 33411024 DOI: 10.1007/s00247-020-04870-3]

4 **Rispo A**, Imperatore N, Testa A, Nardone OM, Luglio G, Caporaso N, Castiglione F. Diagnostic Accuracy of Ultrasonography in the Detection of Postsurgical Recurrence in Crohn's Disease: A Systematic Review with Meta-analysis. *Inflamm Bowel Dis* 2018; **24**: 977-988 [PMID: 29688470 DOI: 10.1093/ibd/izy012]

5 **Paredes JM**, Ripollés T, Cortés X, Moreno N, Martínez MJ, Bustamante-Balén M, Delgado F, Moreno-Osset E. Contrast-enhanced ultrasonography: usefulness in the assessment of postoperative recurrence of Crohn's disease. *J Crohns Colitis* 2013; **7**: 192-201 [PMID: 22542055 DOI: 10.1016/j.crohns.2012.03.017]

6 **Jakob M**, Backes M, Schaefer C, Albert J, Geissler A. MR Enterography in Crohn's Disease: Comparison of Contrast Imaging with Diffusion-weighted Imaging and a special Form of Color Coding. *Rofo* 2022; **194**: 1119-1131 [PMID: 35705164 DOI: 10.1055/a-1826-0049]

7 **Schonberger M**, Lefere P, Dachman AH. Pearls and Pitfalls of Interpretation in CT Colonography. *Can Assoc Radiol J* 2020; **71**: 140-148 [PMID: 32063002 DOI: 10.1177/0846537119892881]

8 **Barat M**, Hoeffel C, Bouquot M, Jannot AS, Dautry R, Boudiaf M, Pautrat K, Kaci R, Camus M, Eveno C, Pocard M, Soyer P, Dohan A. Preoperative evaluation of small bowel complications in Crohn's disease: comparison of diffusion-weighted and contrast-enhanced MR imaging. *Eur Radiol* 2019; **29**: 2034-2044 [PMID: 30302591 DOI: 10.1007/s00330-018-5734-2]

9 **Masselli G**, De Vincentiis C, Aloi M, Guida M, Cao R, Cartocci G, Miele V, Grassi R. Detection of Crohn's disease with diffusion images versus contrast-enhanced images in pediatric using MR enterography with histopathological correlation. *Radiol Med* 2019; **124**: 1306-1314 [PMID: 31317380 DOI: 10.1007/s11547-019-01067-z]

10 **Ma Q**, Xin J, Zhao Z, Guo Q, Yu S, Xu W, Liu C, Zhai W. Value of ^{18}F-FDG PET/CT in the diagnosis of primary gastric cancer *via* stomach distension. *Eur J Radiol* 2013; **82**: e302-e306 [PMID: 23434453 DOI: 10.1016/j.ejrad.2013.01.021]

11 **Lehmann K**, Eshmuminov D, Bauerfeind P, Gubler C, Veit-Haibach P, Weber A, Abdul-Rahman H, Fischer M, Reiner C, Schneider PM. (18)FDG-PET-CT improves specificity of preoperative lymph-node staging in patients with intestinal but not diffuse-type esophagogastric adenocarcinoma. *Eur J Surg Oncol* 2017; **43**: 196-202 [PMID: 27692533 DOI: 10.1016/j.ejso.2016.08.020]

12 **Tsurumaru D**, Nishimuta Y, Muraki T, Asayama Y, Nishie A, Oki E, Honda H. Gastric cancer with synchronous and metachronous hepatic metastasis predicted by enhancement pattern on multiphasic contrast-enhanced CT. *Eur J Radiol* 2018; **108**: 165-171 [PMID: 30396650 DOI:

10.1016/j.ejrad.2018.09.030]

13 **Djuric-Stefanovic A**, Jankovic A, Saponjski D, Micev M, Stojanovic-Rundic S, Cosic-Micev M, Pesko P. Analyzing the post-contrast attenuation of the esophageal wall on routine contrast-enhanced MDCT examination can improve the diagnostic accuracy in response evaluation of the squamous cell esophageal carcinoma to neoadjuvant chemoradiotherapy in comparison with the esophageal wall thickness. *Abdom Radiol (NY)* 2019; **44**: 1722-1733 [PMID: 30758534 DOI: 10.1007/s00261-019-01911-w]

14 **Morani AC**, Gupta S, Elsayes KM, Mubarak AI, Khalaf AM, Bhosale PR, Sun J, Jensen CT, Kundra V. Performance of Multidetector Computed Tomography and Negative Versus Positive Enteric Contrast for Evaluation of Gastrointestinal Neuroendocrine Neoplasms. *J Comput Assist Tomogr* 2022; **46**: 333-343 [PMID: 35575649 DOI: 10.1097/RCT.0000000000001291]

15 **Bi L**, Yang L, Ma J, Cai S, Li L, Huang C, Xu J, Wang X, Huang M. Dynamic contract-enhanced CT-based radiomics for differentiation of pancreatobiliary-type and intestinal-type periampullary carcinomas. *Clin Radiol* 2022; **77**: e75-e83 [PMID: 34753589 DOI: 10.1016/j.crad.2021.09.010]

16 **Ahmetoğlu A**, Cansu A, Baki D, Kul S, Cobanoğlu U, Alhan E, Ozdemir F. MDCT with multiplanar reconstruction in the preoperative local staging of rectal tumor. *Abdom Imaging* 2011; **36**: 31-37 [PMID: 19949791 DOI: 10.1007/s00261-009-9591-y]

17 **Takeda T**, Hayashi S, Kobayashi Y, Tsuji K, Nagai S, Tominaga E, Suzuki T, Okuda S, Banno K, Aoki D. Evaluation of preoperative prediction of intestinal invasion in patients with ovarian cancer. *Int J Gynaecol Obstet* 2021; **153**: 398-404 [PMID: 33222157 DOI: 10.1002/ijgo.13492]

18 **Chen XP**, Liu J, Zhou J, Zhou PC, Shu J, Xu LL, Li B, Su S. Combination of CEUS and MRI for the diagnosis of periampullary space-occupying lesions: a retrospective analysis. *BMC Med Imaging* 2019; **19**: 77 [PMID: 31477041 DOI: 10.1186/s12880-019-0376-7]

19 **Jang KM**, Kim SH, Lee SJ, Park HJ, Choi D, Hwang J. Added value of diffusion-weighted MR imaging in the diagnosis of ampullary carcinoma. *Radiology* 2013; **266**: 491-501 [PMID: 23238154 DOI: 10.1148/radiol.12121106]

20 **Hayoz R**, Vietti-Violi N, Duran R, Knebel JF, Ledoux JB, Dromain C. The combination of hepatobiliary phase with Gd-EOB-DTPA and DWI is highly accurate for the detection and characterization of liver metastases from neuroendocrine tumor. *Eur Radiol* 2020; **30**: 6593-6602 [PMID: 32601948 DOI: 10.1007/s00330-020-06930-6]

21 **Dane B**, Sarkar S, Nazarian M, Galitzer H, O'Donnell T, Remzi F, Chang S, Megibow A. Crohn Disease Active Inflammation Assessment with Iodine Density from Dual-Energy CT Enterography: Comparison with Histopathologic Analysis. *Radiology* 2021; **301**: 144-151 [PMID: 34342502 DOI: 10.1148/radiol.2021204405]

22 **Kotelevets SM**, Chekh SA, Chukov SZ. Updated Kimura-Takemoto classification of atrophic gastritis. *World J Clin Cases* 2021; **9**: 3014-3023 [PMID: 33969087 DOI: 10.12998/wjcc.v9.i13.3014]

23 **Awais M**, Qamar S, Rehman A, Baloch NU, Shafqat G. Accuracy of CT chest without oral contrast for ruling out esophageal perforation using fluoroscopic esophagography as reference standard: a retrospective study. *Eur J Trauma Emerg Surg* 2019; **45**: 517-525 [PMID: 29484462 DOI: 10.1007/s00068-018-0929-4]

24 **Ajlan AM**, Mesurolle B, Stein L, Kao E, Artho G, Al-Rujaib M, Reinhold C. Detectability of choledocholithiasis on CT: The effect of positive intraduodenal enteric contrast on portovenous contrast-enhanced studies. *Saudi J Gastroenterol* 2015; **21**: 306-312 [PMID: 26458858 DOI: 10.4103/1319-3767.164184]

25 **Kim JR**, Suh CH, Yoon HM, Jung AY, Lee JS, Kim JH, Lee JY, Cho YA. Performance of MRI for suspected appendicitis in pediatric patients and negative appendectomy rate: A systematic review and meta-analysis. *J Magn Reson Imaging* 2018; **47**: 767-778 [PMID: 28815859 DOI: 10.1002/jmri.25825]

26 **Chai YR**, Gao JB, Lyu PJ, Liang P, Xing JJ, Liu J. [Comparative study of CT relative enhancement value and subjective visual evaluation for intestinal ischemia in patients with closed loop obstruction]. *Zhonghua Yixue Zazhi* 2021; **101**: 3411-3416 [PMID: 34758545 DOI: 10.3760/cma.j.cn112137-20210328-00756]

27 **Magnusson M**, Malmström EM. The conundrum of cervicogenic dizziness. *Handb Clin Neurol* 2016; **137**: 365-369 [PMID: 27638084 DOI: 10.1016/B978-0-444-63437-5.00026-1]

28 **Chuzhov AL**, Ariél' BM, Bellendir EN, Belkova OV. [Ex juvantibus diagnosis in suspected skin tuberculosis]. *Probl Tuberk Bolezn Legk* 2008; 15-18 [PMID: 19227320]

Published by **Baishideng Publishing Group Inc**
7041 Koll Center Parkway, Suite 160, Pleasanton, CA 94566, USA
Telephone: +1-925-3991568
E-mail: office@baishideng.com
Help Desk: https://www.f6publishing.com/helpdesk
https://www.wjgnet.com